Solvent Organization and Electrostatics Tuned by Solute Electronic Structure: Amide vs. Non-Amide Carbonyls

Steven D.E. Fried,[1] Chu Zheng,[1] Yuezhi Mao,[1] Thomas E. Markland,[1*] and Steven G. Boxer[1*]

[1]Department of Chemistry, Stanford University, Stanford, California 94305, USA

*Corresponding Authors. Emails: tmarkland@stanford.edu; sboxer@stanford.edu

Supporting Information Placeholder

ABSTRACT: The ability to exploit carbonyl groups to measure electric fields in enzymes and other complex reactive environments using the vibrational Stark effect has inspired growing interest in how these fields can be measured, tuned, and ultimately designed. Previous studies have concentrated on the role of the solvent in tuning the fields exerted on the solute. Here, we explore instead the role of the solute electronic structure in modifying the local solvent organization and electric field exerted on the solute. By measuring the infrared absorption spectra of amide-containing molecules, as prototypical peptides, and contrasting them with non-amide carbonyls in a wide range of solvents, we show that these solutes experience notable differences in their frequency shifts in polar solvents. Using vibrational Stark spectroscopy and molecular dynamics simulations, we demonstrate that while some of these differences can be rationalized using the distinct intrinsic Stark tuning rates of the solutes, the larger frequency shifts for amides and dimethylurea primarily result from the larger solvent electric fields experienced by their carbonyl groups. These larger fields arise due to their stronger *p*-π conjugation, which results in larger C=O bond dipole moments that further induce substantial solvent organization. Using electronic structure calculations, we decompose the electric fields into contributions from solvent molecules that are in the first solvation shell and those from the bulk and show that both of these contributions are significant and become larger with enhanced conjugation in solutes. These results show that structural modifications of a solute can be used to tune both the solvent organization and electrostatic environment, indicating the importance of a solute-centric paradigm in modulating and designing the electrostatic environment in condensed-phase chemical processes.

INTRODUCTION

Among fundamental chemical principles, the concept of solvation has long been a topic of significant research, playing a central role in disciplines such as supramolecular chemistry,[1] chemical reactivity,[2] macromolecular folding,[3] and colligative properties of solutions[4]. The molecular properties of both solute and solvent must be simultaneously considered to characterize the solvation process. These properties, which include the total molecular dipole moment and those of individual chemical bonds, the hydrogen bonding donor or acceptor capability, polarizability, and molecular shape, will all influence the types of intermolecular forces between solute and solvent. Each of these interactions will in turn contribute to an overall electric field upon the solute, which can be probed spectroscopically by mapping from the observed frequency shifts using the Stark effect, whether electronic[5-6] or vibrational.[7]

Solute-solvent interactions are frequently analyzed from the perspective of the solvent, where changes to solvent properties (e.g., polarity as characterized by the static dielectric constant ε_s, or polarizability as characterized by the refractive index η) can produce striking changes in solute's absorption spectra, a phenomenon known as solvatochromism.[8-9] Solvatochromism for electronic transitions—the shift of the absorption spectrum due to changes in the solvent polarity—is widely used as a proxy to calibrate solvent polarity.[10] In the case of the vibrational Stark shifts, the changes in frequency can be connected to the electric field induced by the solvent using simulations to generate correlations between the observed frequencies and the calculated fields. This strategy has been successfully employed both for probing solvent fields around small molecules[11-13] as well as in complex and heterogeneous environments such as proteins.[14-18]

While solvatochromism studies have provided significant insights into the role played by the solvent in determining the electric fields experienced by the solute, these fields ultimately arise from the mutual interaction between the solvent and solute, and thus also depend on the fields and structural ordering that the solute exerts on the solvent. These mutual interactions often require a compromise between solvent-solvent interactions and specific solvent-solute interactions such as those arising from charged or dipolar functional groups as well as steric effects.[19-21] Additionally, in some cases there can be a significant interplay between the solvent field and the electronic structure of the solute, such as in donor-acceptor polyenes where changes in solvent polarity lead to drastic changes in the bond-alternation pattern of the polyene.[22-24] Theoretical models that aim to mechanistically understand and predict how solutes direct solvent organization to produce spectroscopic frequency shifts originate with the reaction field model of Onsager,[25] and have since been extended to more detailed self-consistent reaction fields,[26-27] and more recent implicit solvent models.[28-32]

Here we elucidate how the molecular properties of solutes alter the electric fields they experience by investigating and contrasting molecules containing amide (amides and dimethylurea) and non-amide (ester, thioester, and ketone) carbonyls (Figure 1A) in a range of polar solvents. By employing vibrational Stark and infrared (IR) spectroscopies and molecular dynamics (MD) simulations, we show that, of all the carbonyl-containing molecules studied, greater IR frequency shifts and larger fields are directed on carbonyls when nitrogen is included at one or both α-positions. The fields projected on these amide carbonyls are much larger due to the enhanced electron delocalization arising from the *p*-π

conjugation with the adjacent nitrogen atom (Figure 1B), which leads to enhanced carbonyl bond (C=O) dipole moments over non-amides and more pronounced solvent organization about them. The larger fields experienced by amides are important given their biochemical roles in proteins and other natural products,[33] including protein secondary structure determination [34-35] and the synthesis or hydrolysis of peptide bonds in ribosomes or proteases, respectively, which may involve catalysis through electrostatic stabilization of an oxyanion intermediate along the axis of the carbonyl.[36-39]

To gain insights into the underlying mechanism by which the *p*-π conjugation effect in amides tunes the electric field on C=O, we then use electronic structure calculations to quantify the field contributions from solvent molecules in close contact with the solute (e.g., those in the first solvation shell or directly hydrogen-bonded to the solute) and those from the bulk solvents, which are illustrated in Figure 1C. Using water as an example, we demonstrate the existence of a mechanism whereby stronger fields are mediated by increased number of hydrogen bonds (HBs) as well as greater organization of solvent molecules in the bulk, both of which contribute significantly to the field enhancement and increase simultaneously as the solute electronic structure is altered. By doing this, we provide insights into the relative importance of direct solute-solvent interactions and long-range dielectric effects in determining the electric field experienced by the solute, and how these contributions change depending on the solute structure. This offers the opportunity to systematically understand the ways in which solute structures can be modified to tune the solvent organization and the resulting electrostatic environment for chemical processes in condensed-phase systems ranging from solutions to enzymes.

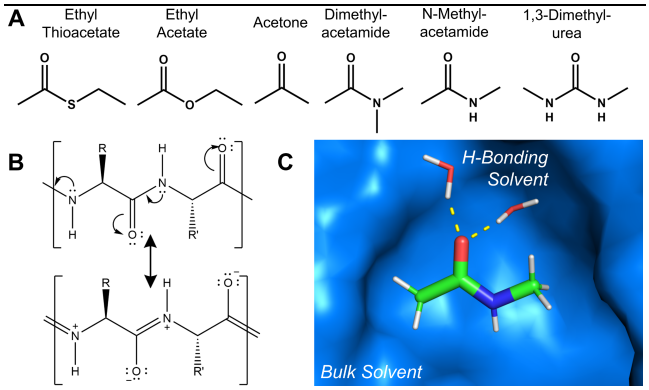

Figure 1. (A) Molecules used in this study. (B) Resonance within a peptide bond via *p*-π conjugation increases the total dipole moment of the amide carbonyl through both charge separation and bond order reduction. (C) Carbonyl-containing solutes such as *N*-methylacetamide (shown with sticks) interact with solvent directly via hydrogen bonds (yellow), and by long-range electrostatic interactions with the bulk dielectric (blue). Both effects contribute to the electric field experienced by the solute carbonyl.

MATERIALS AND METHODS

Materials for Experimental Characterization. The carbonyl-containing compounds were acquired from the following sources: *N,N*-dimethylacetamide (DMA, 99.9%, Sigma-Aldrich), *N*-methylacetamide (NMA, 99%, Sigma-Aldrich), ethyl thioacetate (98%, Sigma-Aldrich), ethyl acetate (99.8%, Sigma-Aldrich), acetone (99.8%, Acros Organics), 1,3-dimethylurea (98%, Acros Organics). Solvents were purchased as follows: 2 methyltetrahydrofuran (2-MeTHF, >99%, Sigma-Aldrich), D_2O (100.0% atom D, Acros Organics), glycer(ol-d3) (99% atom D, Sigma-Aldrich), methanol (99.8%, Fisher Scientific), dimethylsulfoxide (99.7%, Acros Organics), chloroform (99.9%, Acros Organics), dichloromethane (99.9%, Acros Organics), tetrahydrofuran (99.9%, Acros Organics), dibutylether (99%, Sigma-Aldrich), *n*-hexanes (99%, Sigma Aldrich). All reagents were used without further purification.

Vibrational Solvatochromism. All infrared spectra were recorded using a Bruker Vertex 70 FTIR spectrometer with a liquid nitrogen-cooled mercury cadmium telluride (MCT) detector, using previously described methods.[14] A mountable liquid sample cell was constructed from two CaF_2 optical windows (0.75 in diameter, 0.25 in thickness, Red Optronics), separated by two semicircular Teflon (PTFE) spacers (25 and 50 μm thickness), to which 20 μL of sample solution (~ 10 mM) were added. Samples were purged within the instrument by a nitrogen flow for 5 min to remove atmospheric CO_2 and water vapor. Transmission spectra were then recorded by averaging 256 scans between 2000 and 1400 cm^{-1}, each time with 1 cm^{-1} resolution and aperture between 2 and 6 mm to maximize signal intensity without oversaturating the detector. Absorption spectra were calculated by taking the negative logarithm of the transmission spectra and subtracting the spectrum of the blank. Experimental spectra for acetone and 1,3-dimethylurea were compared with previously collected FTIR spectra for dimethylacetamide, ethyl acetate, ethyl thioacetate, and *N*-methylacetamide using similar methods.[17] Each solvatochromism measurement was repeated in triplicate, consistently using three different orientations of the sample cell within the FTIR instrument. Frequencies of the carbonyl stretching band were selected by fitting Gauss-Lorentz curves to the relevant spectral region using the Levenberg-Marquardt algorithm. In cases of closely overlapping peaks, multiple Gauss-Lorentz curves were fitted, with a weighted sum taken based on their respective intensities to identify the ensemble average frequency position.

Vibrational Stark Spectroscopy. Vibrational Stark spectra for ethyl acetate, ethyl thioacetate, *N*-methylacetamide, and dimethylacetamide have been reported by Schneider et al.[17] For this work, acetone and 1,3-dimethylurea were dissolved in glass-forming solvents as indicated with concentrations of 50 mM. Solutions were loaded into a sample cell comprised of two offset CaF_2 windows (1 mm thickness, 12.7 mm diameter, TOCtek Photonics), each coated on the inner face with a 4.5 nm layer of nickel and separated by 26 μm Teflon spacers. Electrodes were connected to each window to convert the sample cell into a parallel-plate capacitor. The filled sample cell was quickly immersed in liquid N_2 in a custom-built cryostat,[40] and Stark spectra were recorded on a Bruker Vertex 70 FTIR spectrometer with fields of $0.5-1.8$ MV/cm (applied voltages of $\sim 1.5-4.0$ kV) from a Trek 10/10 high-voltage power amplifier, using 1 cm^{-1} resolution and 64 scans apiece of field-on/off transmission spectra. Measurements were repeated with increasing fields to ensure that the intensity of the Stark spectrum scales linearly with the square of the field strength as expected for an isotropic, immobilized sample.[41]

The linear Stark tuning rate was determined as previously described by numerically fitting the zeroth, first, and second derivatives of the best-fit Voigt profile of the experimental absorbance spectrum to the Stark spectrum.[41] This analysis assumes an isotropic, immobilized sample and that the angle (ζ) between $|\Delta\vec{\mu}_{C=O}|$ and the transition dipole is zero; the experimentally set angle (χ) between the incident light polarization and the external electric field direction was 90° as previously described (see SI Section I).[41]

In cases where overlapping peaks were observed (e.g., where both hydrogen bonding and non-hydrogen bonding species occur), the derivative contributions were determined from the full absorbance spectrum in the spectral region of interest unless otherwise noted. Note that while the applied electric field ($\vec{F}_{\text{ext}}$) is known accurately from the applied voltage and separation of the electrode, the actual field experienced by the probe ($\vec{F}_{\text{local}}$) differs from this value and needs to be adjusted by a local field correction factor (f), i.e., $\vec{F}_{\text{local}} = f\,\vec{F}_{\text{ext}}$.[41-42] While the exact value of the local field factor is not known (and is treated here as a scaler), it is expected to have a value between 1 and 2 for carbonyls.[7, 13, 16, 43] As such, the Stark tuning rates are reported in terms of $|\Delta\vec{\mu}_{\text{C=O}}|f$; this will be discussed in further detail with the results.

Molecular Dynamics (MD) Simulations. The carbonyl-containing solute molecules were parameterized using Gaussian 16[44] and AmberTools20.[45] The molecules were constructed in GaussView and then geometry-optimized using DFT at the B3LYP/6-311++G(2d,2p) level.[46-47] Optimized solute structures were input into the Antechamber program of AmberTools and parametrized using the General Amber Force Field (GAFF)[48] and the AM1-BCC method[49] to assign fixed atomic charges. Organic solvent parameters were taken from Caleman et al.,[50] while for water the TIP3P model[51] was employed. All MD simulations were set up and performed in GROMACS 2018.[52-53] Each solute was solvated in GROMACS via *gmx solvate* using the benchmarked densities from Caleman et al.[50] in a cubic periodic box of length 40 Å.

The MD simulations were performed with periodic boundary conditions, where long-range electrostatics was treated by particle-mesh-Ewald (PME) with a 1 nm real-space cutoff. The system was first energy-minimized, prior to equilibration in the NVT ensemble for 200 ps at 300 K followed by 200 ps in the NPT ensemble at the same temperature and a pressure of 1 bar. Temperature coupling was controlled with a stochastic velocity-rescaling thermostat,[54] and pressure via the Parrinello-Rahman barostat.[55] MD production runs were carried out for a total of 1 ns, with snapshots of the forces and positions recorded every 200 fs, producing a total of 5,000 snapshots per trajectory. For the calculation of radial distribution functions, the positions were recorded every 2 fs.

Electric Field Calculations. Electric fields acting on the solute carbonyl groups were calculated using both classical force fields and electronic structure calculations at the DFT level. In the first approach, the electric field vectors on the carbon and oxygen atoms were obtained from the electrostatic forces acting on them in each snapshot employing a previously established approach.[14] The total electric field on the carbonyl group was then calculated by averaging the projection of each atom's field vector along the C=O bond direction. Repeating this for each snapshot, the ensemble-averaged value is reported for each solute-solvent combination.

The electric field calculations at the DFT level were performed on the selected MD frames for all six solutes in water using the Q-Chem 5.4.2 software package.[56] The MD frames were first sorted based on the number of hydrogen bonds formed between the carbonyl group and the surrounding water molecules, then 100 frames were randomly selected from each group on which the electronic structure calculations were performed (unless the group contained less than 100 frames, in which case all frames were used). The detailed procedure for DFT-based electric field calculations was elaborated elsewhere.[57] In brief, we first generated truncated solute-solvent clusters with a cutoff radius of 7 Å, i.e., the center-of-mass of each included solvent molecule is within 7 Å of at least one of the solute atoms. We then employed the Subsystem Projection Atomic Orbital Decomposition (SPADE)[58] method to partition the electron density of the entire solute-solvent system, based on DFT calculations at the B3LYP/6-31+G(d) level. The electron density assigned by this partitioning to the solvent part of the system, together with the solvent nuclei, was then used to calculate the electric field vectors on the carbon and oxygen atoms and then the electric field on the carbonyl group.

Hydrogen-bond analysis and decomposition of solvent electric fields. The number of HBs between solute and solvent, plus the angular and distance distributions of those HBs for each solute, were determined using the *gmx hbond* function based on a widely used geometrical criterion for HBs:[59] for the protic solvents (water and methanol), an HB between a solvent O-H group and the solute carbonyl group is defined to occur when the $O_{Solvent}\cdots O_{Solute}$ distance is within 3.5 Å and the $H\text{-}O_{Solvent}\text{-}O_{Solute}$ angle is below 30°. HB interactions to chloroform were identified similarly by a $C_{Solvent}\cdots O_{Solute}$ distance within 4.0 Å, accounting for the longer interaction distances, and a $H\text{-}C_{Solvent}\text{-}O_{Solute}$ angle below 30°.

With water we then quantified the respective contributions from solvent molecules in the first solvation shell (those whose oxygen atoms, O_w, are within 3.5 Å of the carbonyl oxygen, O_c) and from those outside (i.e., bulk solvents). These contributions are referred to as the *inner-* and *outer-shell* contributions to the field, respectively, throughout this paper, and they were obtained from DFT-based electric field calculations with either the outer- or inner-shell water molecules removed from the solute-solvent clusters. An additional non-additive component was then evaluated by subtracting these two contributions from the total electric field acting on C=O, which primarily reflects the effect of mutual polarization between the inner- and outer-shell water molecules. A similar analysis was also performed to determine the field contributions from HB and non-HB water molecules, where the solvent water molecules were categorized based on both the distance and angular criteria for HBs.

RESULTS

Experimental observation of stronger solvent-induced frequency shifts for amides versus non-amides. Figure 2 shows the FTIR spectra obtained for several carbonyl-containing molecules, as an extension of the previous results of Schneider et al.[17] From this it is clear that the relative frequency shifts for the amide-containing molecules (*N*-methylacetamide and 1,3-dimethylurea) are much greater than those observed for acetone: the C=O stretch mode of acetone shifts by only 26 cm^{-1} upon going from the least (hexane) to most polar (water) solvent studied, while that of 1,3-dimethylurea shifts by ~100 cm^{-1}. This is consistent with the previous results showing a similar disparity when comparing the C=O frequency shifts observed for dimethylacetamide to those of ethyl acetate and ethyl thioacetate.[17]

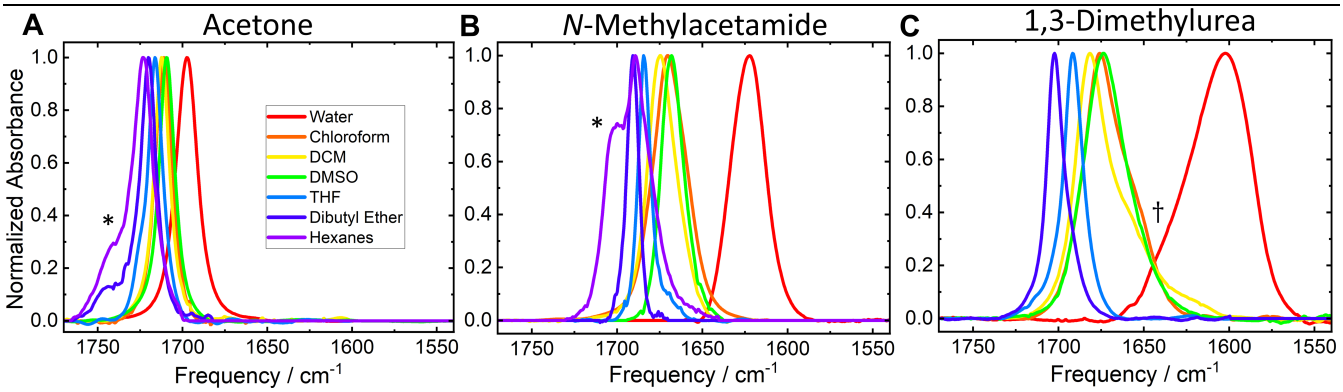

Figure 2. FTIR Spectra of (A) Acetone, (B) *N*-Methylacetamide, and (C) 1,3-Dimethylurea show increasing frequency shifts in more polar solvents. Note that the x-axis scale (in cm^{-1}) is the same in all three panels, making it immediately clear that much larger spectral shifts with solvent polarity are observed for 1,3-dimethylurea than for acetone. Shoulder peaks are presumed to occur due to a dimerizing population in the least polar solvents (*) or Fermi resonances in more polar solvents (†).

To uncover the origin(s) of these striking observations, we consider the interpretation of these results within the framework of the first-order vibrational Stark effect (VSE), which predicts a linear response of infrared absorption frequency to the electric field experienced by the probe oscillator along the axis of its vibrational mode.[7, 12] This is an intrinsic result of the anharmonicity of the oscillator, where the equilibrium bond length d increases upon the transition from the ground to first excited vibrational state. For a polar oscillator with charge separation q, this will entail a change in dipole from $\vec{\mu}_0 = q\vec{d}$ to $\vec{\mu}_1 = q(\vec{d} + \Delta\vec{d})$. Note that in addition to the internal energy of the molecule itself, the electric field arising from a molecule's environment will interact with the oscillator dipole moment to change the total energy in both the ground and excited vibrational states. Hence in the presence of a solvent-induced electric field $\vec{F}$, the IR frequency for a carbonyl will change by $\Delta\bar{\nu}_{C=O} = -\Delta\vec{\mu}_{C=O} \cdot \vec{F} = -|\Delta\vec{\mu}_{C=O}|F_{C=O}$ due to the interaction of the carbonyl difference dipole $\Delta\vec{\mu}_{C=O} = \vec{\mu}_1 - \vec{\mu}_0$ with the field projected onto the carbonyl $F_{C=O}$. Because the carbonyl dipole typically increases upon excitation, such an interaction is energetically favorable when the field from a polar solvent is aligned with the bond direction, leading to a red shift in the vibrational absorption spectrum. Electric fields along the carbonyl can thus be proportionally mapped onto changes in its vibrational frequency according to the Stark tuning rate $|\Delta\vec{\mu}_{C=O}|$. We see that there are two primary factors that can explain the significant difference in $\Delta\bar{\nu}_{C=O}$ for various carbonyls, namely the Stark tuning rate $|\Delta\vec{\mu}_{C=O}|$ as a molecular property associated with the solute electronic structure, and the solvent-induced electric field exerted on the carbonyl bond ($F_{C=O}$). To characterize which property (or combination thereof) is at work in the structure-dependent variation in frequency shifts, we use a combination of experimental and computational means to separately assess both $|\Delta\vec{\mu}_{C=O}|$ and $F_{C=O}$ as well as the factors leading to their variations.

We first consider the role of the Stark tuning rate $|\Delta\vec{\mu}_{C=O}|$ in determining the observed larger amide frequency shifts by performing vibrational Stark spectroscopy (VSS) experiments, where an external electric field is applied to an isotropic immobilized sample in a frozen glass. The resulting changes in the absorption spectra can be used to calibrate the Stark tuning rate.[41] For each molecule investigated by VSS, the Stark spectra we measured are almost entirely dominated by the second derivative of the absorbance spectrum, from which we obtain $|\Delta\vec{\mu}_{C=O}|f$, where f is the local field factor that accounts for the difference between the electric field experienced in the frozen glass and the field applied externally to the sample (see SI section I).[7, 41, 60] For carbonyls the value of f is generally thought to be around 2.[7] The results of the VSS measurements ($|\Delta\vec{\mu}_{C=O}|f$) for each compound are summarized in the second column of Table 1, where the results from this work for acetone and 1,3-dimethylurea (SI Figures S1-S2) are combined with those obtained previously by Schneider et al.[17] The very similar values of $|\Delta\vec{\mu}_{C=O}|f$ shown in Table 1 for NMA in 2-MeTHF and 1:1 Glycer(ol-D_3)-D_2O (both at 1.30 cm^{-1}/(MV/cm)) and those for DMA in 2-MeTHF and ethanol (1.25 vs. 1.26 cm^{-1}/(MV/cm)) suggest that the local field factor changes negligibly with the glass-forming solvent used, at least in these cases.

Table 1 - Vibrational Stark Tuning Rates for Carbonyl-Containing Compounds in Frozen Glasses at 77 K, compared to solvatochromism values

Solute	VSS $\lvert\Delta\mu_{C=O}\rvert f$ cm^{-1}/(MV/cm)	Estimated VSS $\lvert\Delta\mu_{C=O}\rvert$ with $f = 2$ cm^{-1}/(MV/cm)	Solvatochromism $\lvert\Delta\mu_{C=O}\rvert$ cm^{-1}/(MV/cm)
Ethyl thioacetate	1.47 ± 0.01†	0.74	0.55 ± 0.02
Ethyl acetate	1.15†	0.58	0.61 ± 0.04
Acetone	0.74	0.37	0.36 ± 0.03
Dimethylacetamide	1.25†	0.63	0.68 ± 0.06
Dimethylacetamide *in ethanol*	1.26†	0.63	
N-methylacetamide	1.30†	0.65	0.67 ± 0.05
N-methylacetamide *in 1:1 Glycer(ol-D_3)-D_2O*	1.30 ± 0.01†	0.65	
1,3-Dimethylurea	1.24	0.62	1.02 ± 0.03

Values reported originally in this work or (for †) in Ref. [13]. Frozen glass solvents for VSS are 2-methyl tetrahydrofuran unless stated otherwise.

Assuming that the variation in f across these solutes is relatively small, one can use the variations in $|\Delta\vec{\mu}_{C=O}|f$ among these molecules to help explain the observed differences in solvent-induced frequency shifts in Figure 2, which can further be compared with the independently obtained results in the following section using vibrational solvatochromism. In particular, the $|\Delta\vec{\mu}_{C=O}|f$ value of acetone, 0.74 cm^{-1}/(MV/cm), is significantly lower than that of the other molecules, consistent with the observation that its frequency shift due to solvent field is the lowest. On the other hand, variations in $|\Delta\vec{\mu}_{C=O}|f$ alone cannot fully explain the frequency shift differences between the various carbonyl-containing molecules. While $|\Delta\vec{\mu}_{C=O}|f$ for acetone is always between 1/2–2/3 of that of the other molecules, its solvent-induced frequency shifts are substantially smaller (1/4–1/3 of the

others). The amide group has a particularly striking effect: while the amides, ester, thioester, and dimethylurea all have comparable $|\Delta\vec{\mu}_{C=O}|f$ values (Table 1), the solvent-induced frequency shifts of amides, and particularly dimethylurea, are significantly larger, suggesting that their intrinsic Stark tuning rates alone are unable to account for their large frequency shifts. Variations in the Stark tuning rates of these carbonyls due to solvent-induced bond polarization are expected to be insignificant as well.[61-62] Therefore, differences between the solvent electric fields experienced by the amide and non-amide carbonyls should play an even more important role in accounting for the larger solvatochromic shifts of the former, and next we combine the vibrational solvatochromism data and molecular dynamics simulations to investigate how the C=O frequency of each solute varies with the solvent electric field.

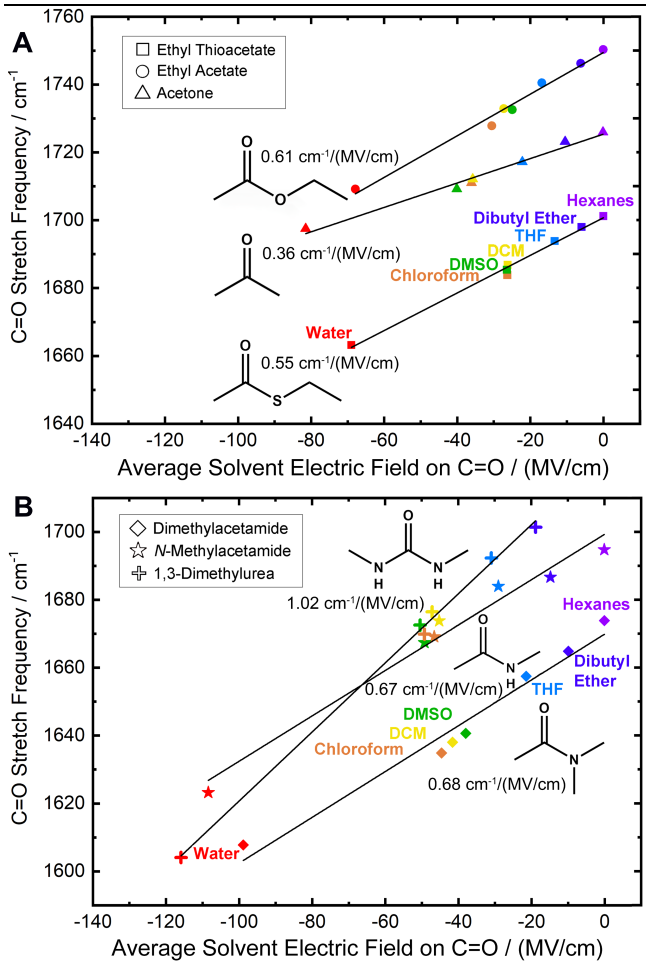

Figure 3. Field-frequency correlation plots for (A) smaller-field carbonyl-containing molecules (ester, thioester, ketone), and (B) larger-field amide and dimethylurea molecules. Here experimentally observed frequencies from FTIR measurements are plotted against the average values of $F_{C=O}$ (i.e., $\langle F_{C=O}\rangle$) calculated using classical force fields in a broad range of solvents. Slopes of the linear correlations (apparent Stark tuning rates $|\Delta\vec{\mu}_{C=O}|$) are provided next to each line, which are characteristically different for acetone and 1,3-dimethylurea (0.36 and 1.02 cm^{-1}/(MV/cm), respectively).

Characterizing Stark tuning rates using vibrational solvatochromism and MD simulations. To understand how the magnitude of electric field on the carbonyl ($F_{C=O}$) varies in different solute-solvent systems, we performed MD simulations of the six solutes in Table 1 in a wide range of solvents of low (hexane) to high (water) polarities and obtained the ensemble-averaged values of $F_{C=O}$ (i.e., $\langle F_{C=O}\rangle$) The variation in the electric fields for the non-amide (Figure 3A) and amide (Figure 3B) carbonyls as the solvent polarity is increased provides significant insights into the observed differences in frequency shifts. The fields projected on C=O are substantially larger for the amide-containing molecules (including dimethylurea) than for the non-amides, by a factor ranging from 1.7 in protic solvents (1,3-dimethylurea vs. ethyl acetate in water) to 3 in certain aprotic solvents (the same two solutes in dibutyl ether). The magnitudes of the fields obtained from simulations show a strong linear correlation with the experimentally observed peak frequency shifts (Figure 3), in keeping with the first-order VSE. The slope in each case gives another estimate for the apparent Stark tuning rates ($|\Delta\vec{\mu}_{C=O}|$), and these values are in good agreement with the VSS values estimated assuming $f = 2$ with the exceptions of ethyl thioacetate and 1,3-dimethylurea (comparing the last two columns in Table 1). For both amides (DMA and NMA) as well as the ester and thioester, the Stark tuning rates obtained from both VSS (using $f = 2$) and solvatochromism data consistently fall in the range of 0.55–0.70 cm^{-1}/(MV/cm). The smaller change in $|\Delta\vec{\mu}_{C=O}|$ across these four solutes (i.e., within a factor of 1.25 from the highest DMA to the lowest ethyl thioacetate) compared to the variation in solvatochromic shifts going from hexane to water (differing by a factor of ~1.75 between DMA and ethyl thioacetate) suggests that the amide-containing solutes are able to induce solvent organization about them to enhance the electric field that stabilizes the carbonyl.

Increased solvent organization around amide solutes and the effects on calculated electric fields. We now aim to correlate the structural properties of the solvents and solutes with the observed electric fields. As shown in SI Figure S3, the first solvation peak in the radial distribution functions (RDFs) of each simulated solvent about the solute carbonyl oxygen is notably more pronounced for the amides and 1,3-dimethylurea than for the other solutes, while the peak position, r_{max}, stays essentially invariant for a given solvent regardless of the solute (Figure 4A, SI Figure S3). This holds for all three solvents studied here that can form HBs with the carbonyls: water, methanol ($r_{max} \approx 2.7$ Å for both), and chloroform ($r_{max} \approx 3.3$ Å). The similar first solvation peak positions for these solutes in each solvent but distinct amplitudes suggest that the number of HBs (n_{HB}) formed by each solute carbonyl towards HB-donor solvents may account for the differences in the electric fields they experience. We confirm this trend by demonstrating the linear correlation between the ensemble-averaged value of n_{HB} ($\langle n_{HB}\rangle$) and the magnitude of $\langle F_{C=O}\rangle$in three solvents: water, methanol, and chloroform. The variation in $\langle n_{HB}\rangle$ for the different solutes can be seen to correlate strongly with the AM1-BCC partial charges on their carbonyl oxygens that were assigned via AmberTools for the MD simulations (Figure 4B).[49] The higher charges and hence larger bond dipoles of the amide carbonyls, as obtained from DFT calculations in vacuum and in the force fields employed (where the fixed charges were also assigned based on electronic structure calculations), arise from the larger extent of p-π conjugation in these molecules, which in solution allow them to induce stronger organization of the solvent molecules nearby. As shown in Figure 4, the greatest changes in $\langle n_{HB}\rangle$ and $\langle F_{C=O}\rangle$ occur between the ketone (acetone) and the first amide (DMA), and to a lesser extent between the amides and 1,3-dimethylurea (the latter has one additional sp^2-nitrogen in conjugation with the carbonyl). In the case of ethyl acetate and ethyl thioacetate, the conjugation effects are insignificant due to the high electronegativity of oxygen and higher shell number of sulfur, respectively, leading to lesser changes to the polarity of their carbonyl groups.

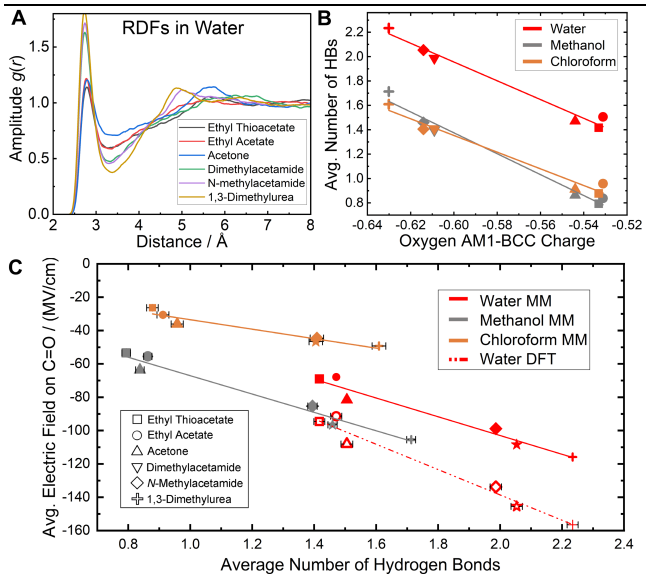

Figure 4. (A) Radial distribution functions (RDFs) describing distance distribution between O_w in water and the carbonyl oxygen in six various solutes. (B) Linear correlation between the AM1-BCC partial charges on the carbonyl oxygen (O_c) used in the simulations and the average number of HBs formed to the carbonyl for the same six solutes in three HB-forming solvents: water, methanol, and chloroform. (C) Linear correlation between the average electric field experienced by the solute carbonyl and the average number of HBs it forms in the three HB-forming solvents. The electric fields are calculated by classical molecular mechanics (MM) force fields for each of the solvents, and additionally by DFT in the case of water.

The results in Figure 4 thus indicate that the substantial increase in $\langle n_{\mathrm{HB}} \rangle$ (e.g., from 1.42 (ethyl thioacetate) to 2.23 (1,3-dimethylurea) in water) leads to a larger solvent electric field on the carbonyls of these solutes. On the other hand, as shown in the correlations between n_{HB} and $\langle F_{\mathrm{C=O}} \rangle$ for each individual solute within a single MD trajectory (SI Figures S4 and S5), the electric fields will still be on average negative (stabilizing) for those frames where $n_{\mathrm{HB}} = 0$, indicating a sizeable contribution that does not just arise from the HB solvent molecules in the first coordination shell. To further investigate the molecular details, we then employ electronic structure calculations to decompose the total solvent electric fields into direct HB and bulk components (Figure 1C) and demonstrate how each of them depends on n_{HB}.

Decomposing the solvent electric fields experienced by carbonyls in different hydrogen bonding environments. We employed DFT calculations to quantify the respective contributions to the electric fields on solute carbonyls ($\langle F_{\mathrm{C=O}} \rangle$) in water from solvent molecules within the first coordination shell ($r_{\mathrm{O_wO_c}} \leq 3.5$ Å, where O_w and O_c denote the water and carbonyl oxygens, respectively) and from those outside ($r_{\mathrm{O_wO_c}} > 3.5$ Å) in different HB environments as characterized using the n_{HB} value of each configuration. Note that DFT gives larger fields than those obtained from the employed force field (see the red solid and patterned lines in Figure 4C) because of its ability to capture phenomena like solvent polarization. Nevertheless, since DFT systematically increases the field strength for each solute-solvent system by ~30 MV/cm, it only slightly affects the apparent Stark tuning rates which depend only on the slopes of the field-frequency correlations. Figures 5A and 5B show the variations of the inner- and outer-shell field contributions with n_{HB}, respectively. The magnitudes of the inner-shell contributions increase approximately linearly with n_{HB}. For each solvent, slight curvature towards saturation of field strength with higher n_{HB} (3 and 4) arises from the decrease in the field contribution per HB as more HBs are formed due to the increasingly crowded first coordination shell (i.e., shift of the $r_{\mathrm{O_wO_c}}$ distribution to longer distances for configurations with larger n_{HB}, SI Figure S6). While the inner- and outer-shell waters together contribute to ~95% of the total field, the remaining contribution arises from the mutual polarization between the solvation shells, which makes the field on C=O even more stabilizing (Figure 5A).

Figure 5C shows the average contributions from the inner- and outer-shell water molecules as well as the mutual polarization between them for all six solutes, which are obtained by weighting the $\langle F_{\mathrm{C=O}} \rangle$ values of each solute (as shown in Figures 5A and 5B) by their characteristic population of each n_{HB} group (SI Table S1). While for all the solutes the inner-shell waters make the largest contribution to the field accounting for 68-81% of the total, there is also a significant contribution from the outer-shells ranging from 14% to 27%. This notable electric field contribution from the outer-shell may likewise extend to functionally important electrostatic interactions in proteins, considering both the HB interactions in the short range[16, 63-64] and the overall charge distribution of the protein.[65-66] Figure 5C also shows that the magnitudes of both the inner- and outer-shell contributions to $\langle F_{\mathrm{C=O}} \rangle$ are markedly larger for amide-containing solutes (DMA, NMA, and 1,3-dimethylurea). The larger inner-shell contributions for the amides arises from their propensity to form more HBs than non-amides (i.e., they have on average higher n_{HB} values, see SI Tables S1 and S6), and their individual HBs also turn out to be stronger on average due to enhanced solute-solvent polarization. For example, going from acetone to 1,3-dimethylurea, the change in the total inner-shell solvent electric field (32.7 MV/cm) is partially attributed to a shift in the distribution of n_{HB}, which accounts for 16.0 MV/cm of the field difference. This estimate is based on the linear correlation relating n_{HB} to the inner-shell field contribution (Figure 5A), i.e., we substituted the $\langle n_{\mathrm{HB}} \rangle$ values of acetone (1.505) and 1,3-dimethylurea (2.234) into the fitted linear correlation for acetone ($F_{\mathrm{C=O}}^{\mathrm{in}} = -23.542\, n_{\mathrm{HB}} + 37.321, R^2 = 0.991$) and then evaluated the difference between the resulting fields. The remaining 16.7 MV/cm difference in solvent-induced field on these two solutes is then attributed to the enhancement of field contributed by individual HBs. Note that this increase in individual HB's field contribution is expected to be more pronounced with fields calculated using DFT, since in QM calculations the inner-shell solvent molecules can be strongly polarized by the solute, an effect that is not captured by the fixed-charge MM calculations. In terms of the outer-shell contributions to $\langle F_{\mathrm{C=O}} \rangle$, the particularly large values for NMA and 1,3-dimethylurea are consistent with the increased ordering of the second coordination shell as observed in their $O_w \cdots O_c$ RDFs (SI Figure S3).

Figures 5A and 5B demonstrate that our solvent electric field decomposition scheme using DFT is able to successfully separate the field into an n_{HB}-dependent inner-shell component ($r_{\mathrm{O_wO_c}} \leq 3.5$ Å) and an n_{HB}-independent outer-shell component ($r_{\mathrm{O_wO_c}} > 3.5$ Å). In contrast, one could additionally invoke a commonly employed angular cutoff for HBs ($\angle$H-O_w-O_c < 30°), which combines the water molecules in the first solvation shell that do not meet the angular criterion, yet have strong HB character, with the outer-shell ones (see SI Figure S7A for the average populations of the first solvation shell by HB and non-HB waters; Figure S7B for the distribution of $\angle$H-O_w-O_c for each solute). However, in doing so we find a strong dependence of the bulk (non-HB) contribution to

the field on n_{HB}, which then inversely correlates with the HB component of the field (see SI Figure S8). This demonstrates that even geometrically distorted HBs (those with ∠H-O_w-O_c > 30°) that fall radially within the first solvation shell ($r_{O_wO_c} \leq 3.5$ Å) make a significant contribution to the field.

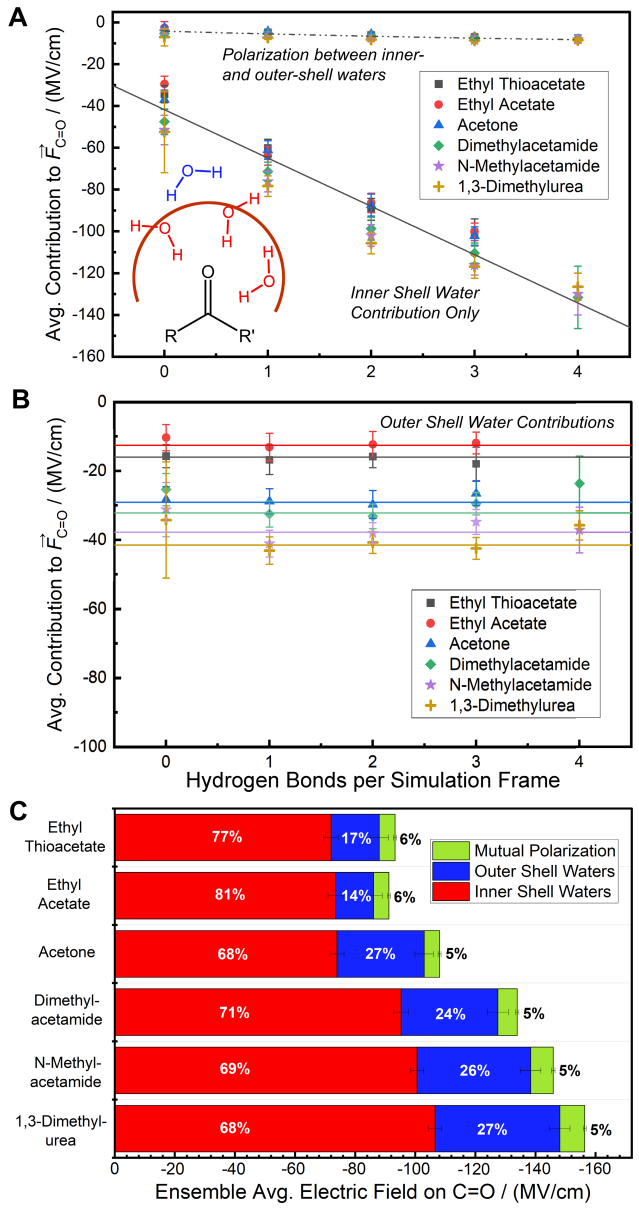

Figure 5. Separation of contributions to the overall electric field on carbonyls ($\langle|F_{C=O}|\rangle$) for six solute molecules based on DFT calculations. (A) Electric field contributions arising from waters in the first solvation shell (up to 3.5 Å from the carbonyl oxygen, solid line) and the component of the overall field describing the polarization between inner- and outer-shell waters (patterned line), where linear models are fitted through the plotted points (average fields from up to 100 snapshots for each n_{HB}) collectively to guide the eye. (B) Field contributions from outer-shell solvent water molecules, where the solid lines indicate ensemble-averaged outer-shell contributions to the field on each solute. (C) Ensemble-averaged electric field for each of the six carbonyl-containing solutes, with the absolute strengths and percentage weights of the inner-shell, outer-shell, and mutual polarization components depicted.

CONCLUSIONS

Using a combined experimental and computational approach, we have demonstrated in this work that amide carbonyl groups are subjected to substantially larger electric fields arising from polar solvent environments, which can be nearly twice as strong as those on non-amide carbonyls, such as ketones, esters, and thioesters. This gives rise to the markedly larger vibrational solvatochromic shifts of the amide-containing compounds. Our MD simulations for a wide variety of solute-solvent systems show that amide carbonyls induce more pronounced solvent organizations around them, as indicated by their more prominent first solvation peaks in the RDFs and the larger average number of HBs they form in protic solvents than non-amides, giving rise to the more substantial electric fields they experience in solution. This ability of the amide-containing solutes to induce local solvent ordering originates from the substantial *p*-π conjugation between the amide sp^2-nitrogens and the carbonyl groups, which increases the polarity of the amide C=O bonds. By employing a scheme based on DFT calculations, we demonstrated that one can decompose the total solvent electric field exerted on C=O into contributions from the inner- and outer-shell solvent molecules, which show strong and little dependence on the number of HBs, respectively. Performing this decomposition for all six solutes in water reveals that the larger electric fields experienced by the amide carbonyls arise from a combination of their propensity to form more HBs, the enhanced field contribution per HB, and their larger field contributions from solvent molecules in the bulk. In contrast to previous studies that have correlated the large frequency shifts of amide carbonyls in water with the lengths of HBs they form[62, 67] or the electron-donating ability of the C=O groups,[68] our results show that the magnitude of these solvatochromic shifts are determined by the electrostatic environments and can be quantitatively mapped from a simple physical descriptor, i.e., the projection of solvent electric field along the C=O bond, based on the linear vibrational Stark effect.

Our findings further substantiate the electrostatic model where solvent molecules organize themselves to stabilize solute bond dipoles[57] and suggest approaches to modulate the electrostatic environment experienced by a solute via modifying its own molecular structure. Such an understanding provides an important implication for the design of new vibrational Stark probes, that is, these probes should minimally perturb the environment so that they can be employed for *in-situ* measurements of electric fields in complex environments. Furthermore, in biological catalysis it has been suggested that preorganized electrostatic environments in the active sites of enzymes play a central role in their catalytic functionality,[16, 34, 69] a principle that has been used to guide the design of mutated enzymes as well as biomimetic catalysts. The multiple effects that lead to the greater electric fields experienced by amide carbonyls described in this work, on the other hand, suggest the possibility of an alternative substrate (solute)-centric approach to achieving electrostatic environments that are favorable to catalysis, i.e., one can induce preorganization in the environment by introducing chemically inert but electrostatically consequential structural motifs to the substrate.[70] Our combined experimental and computational approaches employed in this work will provide a route to elucidating the physics underlying these electrostatics-inspired strategies for catalyst design.

ASSOCIATED CONTENT

* Supporting Information

The Supporting Information is available free of charge on the ACS Publication Website.

AUTHOR INFORMATION

Notes

The authors declare no competing financial interest.

ACKNOWLEDGMENTS

This work was supported in part by grants from the National Science Foundation Grant Nos. MCB-1915727 (to S.G.B) and CHE-2154291 (to T.E.M), as well as National Institutes of Health Grant R35GM118044 (to S.G.B). S.D.E.F is supported by the NSF Graduate Research Fellowship under Grant No. DGE-1656518, C.Z. is supported the Stanford Center for Molecular Analysis and Design (CMAD) Fellowship, and T.E.M. also acknowledges support from the Camille Dreyfus Teacher-Scholar Awards Program. This research also used resources of the National Energy Research Scientific Computing Center (NERSC), a U.S. Department of Energy Office of Science User Facility operated under Contract No. DE-AC02-05CH11231, and the Sherlock cluster operated by the Stanford Research Computing Center.

REFERENCES

1. Mabesoone, M. F. J.; Palmans, A. R. A.; Meijer, E. W., Solute–Solvent Interactions in Modern Physical Organic Chemistry: Supramolecular Polymers as a Muse. *J. Am. Chem. Soc.* **2020,** *142* (47), 19781-19798.
2. Reichardt, C.; Welton, T., *Solvents and Solvent Effects in Organic Chemistry*. 4th ed.; John Wiley & Sons: 2011.
3. Davis, C. M.; Gruebele, M.; Sukenik, S., How does solvation in the cell affect protein folding and binding? *Curr. Opin. Struct. Biol.* **2018,** *48*, 23-29.
4. Wilson, A. D.; Stetson, C., Modeling solution vapor equilibria with solvation and solute assembly. *J. Mol. Liq.* **2021,** *336*, 116272.
5. Donon, J.; Habka, S.; Vaquero-Vara, V.; Brenner, V.; Mons, M.; Gloaguen, E., Electronic Stark Effect in Isolated Ion Pairs. *J. Phys. Chem. Lett.* **2019,** *10* (23), 7458-7462.
6. Lin, C.-Y.; Romei, M. G.; Oltrogge, L. M.; Mathews, I. I.; Boxer, S. G., Unified Model for Photophysical and Electro-Optical Properties of Green Fluorescent Proteins. *J. Am. Chem. Soc.* **2019,** *141* (38), 15250-15265.
7. Fried, S. D.; Boxer, S. G., Measuring Electric Fields and Noncovalent Interactions Using the Vibrational Stark Effect. *Acc. Chem. Res.* **2015,** *48* (4), 998-1006.
8. Andrews, S. S.; Boxer, S. G., Vibrational Stark Effects of Nitriles II. Physical Origins of Stark Effects from Experiment and Perturbation Models. *J. Phys. Chem. A* **2002,** *106* (3), 469-477.
9. Cho, M., Vibrational solvatochromism and electrochromism: Coarse-grained models and their relationships. *J. Chem. Phys.* **2009,** *130* (9), 094505.
10. Reichardt, C., Solvatochromic Dyes as Solvent Polarity Indicators. *Chem. Rev.* **1994,** *94* (8), 2319-2358.
11. Choi, J.-H.; Cho, M., Vibrational solvatochromism and electrochromism of infrared probe molecules containing C≡O, C≡N, C=O, or C−F vibrational chromophore. *J. Chem. Phys.* **2011,** *134* (15), 154513.
12. Levinson, N. M.; Fried, S. D.; Boxer, S. G., Solvent-Induced Infrared Frequency Shifts in Aromatic Nitriles Are Quantitatively Described by the Vibrational Stark Effect. *J. Phys. Chem. B* **2012,** *116* (35), 10470-10476.
13. Fried, S. D.; Wang, L.-P.; Boxer, S. G.; Ren, P.; Pande, V. S., Calculations of the Electric Fields in Liquid Solutions. *J. Phys. Chem. B* **2013,** *117* (50), 16236-16248.
14. Fried, S. D.; Bagchi, S.; Boxer, S. G., Measuring Electrostatic Fields in Both Hydrogen-Bonding and Non-Hydrogen-Bonding Environments Using Carbonyl Vibrational Probes. *J. Am. Chem. Soc.* **2013,** *135* (30), 11181-11192.
15. Liu, C. T.; Layfield, J. P.; Stewart, R. J.; French, J. B.; Hanoian, P.; Asbury, J. B.; Hammes-Schiffer, S.; Benkovic, S. J., Probing the Electrostatics of Active Site Microenvironments along the Catalytic Cycle for Escherichia coli Dihydrofolate Reductase. *J. Am. Chem. Soc.* **2014,** *136* (29), 10349-10360.
16. Fried, S. D.; Bagchi, S.; Boxer, S. G., Extreme electric fields power catalysis in the active site of ketosteroid isomerase. *Science* **2014,** *346* (6216), 1510-1514.
17. Schneider, S. H.; Boxer, S. G., Vibrational Stark Effects of Carbonyl Probes Applied to Reinterpret IR and Raman Data for Enzyme Inhibitors in Terms of Electric Fields at the Active Site. *J. Phys. Chem. B* **2016,** *120* (36), 9672-9684.
18. Schneider, S. H.; Kozuch, J.; Boxer, S. G., The Interplay of Electrostatics and Chemical Positioning in the Evolution of Antibiotic Resistance in TEM β-Lactamases. Cold Spring Harbor Laboratory: 2021.
19. Lum, K.; Chandler, D.; Weeks, J. D., Hydrophobicity at Small and Large Length Scales. *J. Phys. Chem. B* **1999,** *103* (22), 4570-4577.
20. Tanford, C.; Kirkwood, J. G., Theory of protein titration curves. I. General equations for impenetrable spheres. *J. Am. Chem. Soc.* **1957,** *79* (20), 5333-5339.
21. Patel, A. J.; Varilly, P.; Jamadagni, S. N.; Acharya, H.; Garde, S.; Chandler, D., Extended surfaces modulate hydrophobic interactions of neighboring solutes. *Proc. Natl. Acad. Sci. U. S. A.* **2011,** *108* (43), 17678.
22. Gorman, C. B.; Marder, S. R., An investigation of the interrelationships between linear and nonlinear polarizabilities and bond-length alternation in conjugated organic molecules. *Proc. Natl. Acad. Sci. U. S. A.* **1993,** *90* (23), 11297.
23. Marder, S. R.; Perry, J. W.; Tiemann, B. G.; Gorman, C. B.; Gilmour, S.; Biddle, S. L.; Bourhill, G., Direct observation of reduced bond-length alternation in donor/acceptor polyenes. *J. Am. Chem. Soc.* **1993,** *115* (6), 2524-2526.
24. Bublitz, G. U.; Ortiz, R.; Marder, S. R.; Boxer, S. G., Stark Spectroscopy of Donor/Acceptor Substituted Polyenes. *J. Am. Chem. Soc.* **1997,** *119* (14), 3365-3376.
25. Onsager, L., Electric Moments of Molecules in Liquids. *J. Am. Chem. Soc.* **1936,** *58* (8), 1486-1493.
26. Tapia, O.; Goscinski, O., Self-consistent reaction field theory of solvent effects. *Mol. Phys.* **1975,** *29* (6), 1653-1661.
27. Marten, B.; Kim, K.; Cortis, C.; Friesner, R. A.; Murphy, R. B.; Ringnalda, M. N.; Sitkoff, D.; Honig, B., New Model for Calculation of Solvation Free Energies: Correction of Self-Consistent Reaction Field Continuum Dielectric Theory for Short-Range Hydrogen-Bonding Effects. *J. Phys. Chem.* **1996,** *100* (28), 11775-11788.
28. Marenich, A. V.; Cramer, C. J.; Truhlar, D. G., Universal Solvation Model Based on Solute Electron Density and on a Continuum Model of the Solvent Defined by the Bulk Dielectric Constant and Atomic Surface Tensions. *J. Phys. Chem. B* **2009,** *113* (18), 6378-6396.
29. Herbert, J. M., Dielectric continuum methods for quantum chemistry. *Comput. Mol. Sci.* **2021,** *11* (4), e1519.
30. Mennucci, B., Polarizable continuum model. *Comput. Mol. Sci.* **2012,** *2* (3), 386-404.
31. Tomasi, J.; Mennucci, B.; Cammi, R., Quantum Mechanical Continuum Solvation Models. *Chem Rev* **2005,** *105* (8), 2999-3094.
32. Hille, C.; Ringe, S.; Deimel, M.; Kunkel, C.; Acree, W. E.; Reuter, K.; Oberhofer, H., Generalized molecular solvation in non-aqueous solutions by a single parameter implicit solvation scheme. *J. Chem. Phys.* **2019,** *150* (4), 041710.
33. Gersch, M.; Kreuzer, J.; Sieber, S. A., Electrophilic natural products and their biological targets. *Nat. Prod. Rep.* **2012,** *29* (6), 659.
34. Warshel, A.; Russell, S. T., Calculations of electrostatic interactions in biological systems and in solutions. *Q. Rev. Biophys.* **1984,** *17* (3), 283-422.
35. Wang, X.; Li, Y.; He, X.; Chen, S.; Zhang, J. Z. H., Effect of Strong Electric Field on the Conformational Integrity of Insulin. *J. Phys. Chem. A* **2014,** *118* (39), 8942-8952.
36. Phillips, M. A.; Fletterick, R.; Rutter, W. J., Arginine 127 stabilizes the transition state in carboxypeptidase. *J. Biol. Chem.* **1990,** *265* (33), 20692-20698.
37. Nicolas, A.; Egmond, M.; Verrips, C. T.; De Vlieg, J.; Longhi, S.; Cambillau, C.; Martinez, C., Contribution of Cutinase Serine 42 Side Chain to the Stabilization of the Oxyanion Transition State. *Biochemistry* **1996,** *35* (2), 398-410.

38. Schmeing, T. M.; Huang, K. S.; Kitchen, D. E.; Strobel, S. A.; Steitz, T. A., Structural Insights into the Roles of Water and the 2′ Hydroxyl of the P Site tRNA in the Peptidyl Transferase Reaction. *Mol. Cell* **2005,** *20* (3), 437-448.
39. Wallin, G.; Åqvist, J., The transition state for peptide bond formation reveals the ribosome as a water trap. *Proc. Natl. Acad. Sci. U. S. A.* **2010,** *107* (5), 1888-1893.
40. Andrews, S. S.; Boxer, S. G., A liquid nitrogen immersion cryostat for optical measurements. *Rev. Sci. Instrum.* **2000,** *71* (9), 3567-3569.
41. Bublitz, G. U.; Boxer, S. G., Stark Spectroscopy: Applications in Chemistry, Biology, and Materials Science. *Annu. Rev. Phys. Chem.* **1997,** *48* (1), 213-242.
42. Andrews, S. S.; Boxer, S. G., Vibrational Stark Effects of Nitriles I. Methods and Experimental Results. *J. Phys. Chem. A* **2000,** *104* (51), 11853-11863.
43. Davari, N.; Daub, C. D.; Åstrand, P.-O.; Unge, M., Local Field Factors and Dielectric Properties of Liquid Benzene. *J. Phys. Chem. B* **2015,** *119* (35), 11839-11845.
44. Frisch, M. J.; Trucks, G. W.; Schlegel, H. B.; Scuseria, G. E.; Robb, M. A.; Cheeseman, J. R.; Scalmani, G.; Barone, V.; Petersson, G. A.; Nakatsuji, H.; Li, X.; Caricato, M.; Marenich, A. V.; Bloino, J.; Janesko, B. G.; Gomperts, R.; Mennucci, B.; Hratchian, H. P.; Ortiz, J. V.; Izmaylov, A. F.; Sonnenberg, J. L.; Williams-Young, D.; Ding, F.; Lipparini, F.; Egidi, F.; Goings, J.; Peng, B.; Petrone, A.; Henderson, T.; Ranasinghe, D.; Zakrzewski, V. G.; Gao, J.; Rega, N.; Zheng, G.; Liang, W.; Hada, M.; Ehara, M.; Toyota, K.; Fukuda, R.; Hasegawa, J.; Ishida, M.; Nakajima, T.; Honda, Y.; Kitao, O.; Nakai, H.; Vreven, T.; Throssell, K.; J. A. Montgomery, J.; Peralta, J. E.; Ogliaro, F.; Bearpark, M.; Heyd, J. J.; Brothers, E. N.; Kudin, K. N.; Staroverov, V. N.; Kobayashi, R.; Normand, J.; Raghavachari, K.; Rendell, A. P.; Burant, J. C.; Iyengar, S. S.; Tomasi, J.; Cossi, M.; Rega, N.; Millam, J. M.; Klene, M.; Adamo, C.; Cammi, R.; Ochterski, J. W.; Martin, R. L.; Morokuma, K.; Farkas, O.; Foresman, J. B.; Fox, D. J. *Gaussian 16, Revision A.03*, Gaussian, Inc.: Wallingford CT, 2016.
45. Case, D. A.; Belfon, K.; Ben-Shalom, I. Y.; Brozell, S. R.; Cerutti, D. S.; T.E. Cheatham, I.; Cruzeiro, V. W. D.; Darden, T. A.; Duke, R. E.; Giambasu, G.; Gilson, M. K.; Gohlke, H.; Goetz, A. W.; Harris, R.; Izadi, S.; Izmailov, S. A.; Kasavajhala, K.; Kovalenko, A.; Krasny, R.; Kurtzman, T.; Lee, T. S.; LeGrand, S.; Li, P.; Lin, C.; Liu, J.; Luchko, T.; Luo, R.; Man, V.; Merz, K. M.; Miao, Y.; Mikhailovskii, O.; Monard, G.; Nguyen, H.; Onufriev, A.; Pan, F.; Pantano, S.; Qi, R.; Roe, D. R.; Roitberg, A.; Sagui, C.; Schott-Verdugo, S.; Shen, J.; Simmerling, C. L.; Skrynnikov, N. R.; Smith, J.; Swails, J.; Walker, R. C.; Wang, J.; Wilson, L.; Wolf, R. M.; Wu, X.; Xiong, Y.; Xue, Y.; York, D. M.; Kollman, P. A. *AMBER 2020*, University of California, San Francisco, 2020.
46. Krishnan, R.; Binkley, J. S.; Seeger, R.; Pople, J. A., Self‐consistent molecular orbital methods. XX. A basis set for correlated wave functions. *J. Chem. Phys.* **1980,** *72* (1), 650-654.
47. Stephens, P. J.; Devlin, F. J.; Chabalowski, C. F.; Frisch, M. J., Ab Initio Calculation of Vibrational Absorption and Circular Dichroism Spectra Using Density Functional Force Fields. *J. Chem. Phys.* **1994,** *98* (45), 11623-11627.
48. Wang, J.; Wolf, R. M.; Caldwell, J. W.; Kollman, P. A.; Case, D. A., Development and testing of a general amber force field. *J. Comput. Chem.* **2004,** *25* (9), 1157-1174.
49. Jakalian, A.; Jack, D. B.; Bayly, C. I., Fast, efficient generation of high-quality atomic charges. AM1-BCC model: II. Parameterization and validation. *J. Comput. Chem.* **2002,** *23* (16), 1623-1641.
50. Caleman, C.; van Maaren, P. J.; Hong, M.; Hub, J. S.; Costa, L. T.; van der Spoel, D., Force Field Benchmark of Organic Liquids: Density, Enthalpy of Vaporization, Heat Capacities, Surface Tension, Isothermal Compressibility, Volumetric Expansion Coefficient, and Dielectric Constant. *J. Chem. Theory Comput.* **2012,** *8* (1), 61-74.
51. Jorgensen, W. L.; Chandrasekhar, J.; Madura, J. D.; Impey, R. W.; Klein, M. L., Comparison of simple potential functions for simulating liquid water. *J. Chem. Phys.* **1983,** *79* (2), 926-935.
52. Abraham, M. J.; Spoel, D. v. d.; Lindahl, E.; Hess, B.; team, t. G. d. *GROMACS User Manual version 2018*, www.gromacs.org: 2018.
53. Abraham, M. J.; Murtola, T.; Schulz, R.; Páll, S.; Smith, J. C.; Hess, B.; Lindahl, E., GROMACS: High performance molecular simulations through multi-level parallelism from laptops to supercomputers. *SoftwareX* **2015,** *1-2*, 19-25.
54. Bussi, G.; Donadio, D.; Parrinello, M., Canonical sampling through velocity rescaling. *J. Chem. Phys.* **2007,** *126* (1), 014101.
55. Parrinello, M.; Rahman, A., Polymorphic transitions in single crystals: A new molecular dynamics method. *J. App. Phys.* **1981,** *52* (12), 7182-7190.
56. Epifanovsky, E.; Gilbert, A. T. B.; Feng, X.; Lee, J.; Mao, Y.; Mardirossian, N.; Pokhilko, P.; White, A. F.; Coons, M. P.; Dempwolff, A. L.; Gan, Z.; Hait, D.; Horn, P. R.; Jacobson, L. D.; Kaliman, I.; Kussmann, J.; Lange, A. W.; Lao, K. U.; Levine, D. S.; Liu, J.; McKenzie, S. C.; Morrison, A. F.; Nanda, K. D.; Plasser, F.; Rehn, D. R.; Vidal, M. L.; You, Z.-Q.; Zhu, Y.; Alam, B.; Albrecht, B. J.; Aldossary, A.; Alguire, E.; Andersen, J. H.; Athavale, V.; Barton, D.; Begam, K.; Behn, A.; Bellonzi, N.; Bernard, Y. A.; Berquist, E. J.; Burton, H. G. A.; Carreras, A.; Carter-Fenk, K.; Chakraborty, R.; Chien, A. D.; Closser, K. D.; Cofer-Shabica, V.; Dasgupta, S.; de Wergifosse, M.; Deng, J.; Diedenhofen, M.; Do, H.; Ehlert, S.; Fang, P.-T.; Fatehi, S.; Feng, Q.; Friedhoff, T.; Gayvert, J.; Ge, Q.; Gidofalvi, G.; Goldey, M.; Gomes, J.; González-Espinoza, C. E.; Gulania, S.; Gunina, A. O.; Hanson-Heine, M. W. D.; Harbach, P. H. P.; Hauser, A.; Herbst, M. F.; Hernández Vera, M.; Hodecker, M.; Holden, Z. C.; Houck, S.; Huang, X.; Hui, K.; Huynh, B. C.; Ivanov, M.; Jász, Á.; Ji, H.; Jiang, H.; Kaduk, B.; Kähler, S.; Khistyaev, K.; Kim, J.; Kis, G.; Klunzinger, P.; Koczor-Benda, Z.; Koh, J. H.; Kosenkov, D.; Koulias, L.; Kowalczyk, T.; Krauter, C. M.; Kue, K.; Kunitsa, A.; Kus, T.; Ladjánszki, I.; Landau, A.; Lawler, K. V.; Lefrancois, D.; Lehtola, S.; Li, R. R.; Li, Y.-P.; Liang, J.; Liebenthal, M.; Lin, H.-H.; Lin, Y.-S.; Liu, F.; Liu, K.-Y.; Loipersberger, M.; Luenser, A.; Manjanath, A.; Manohar, P.; Mansoor, E.; Manzer, S. F.; Mao, S.-P.; Marenich, A. V.; Markovich, T.; Mason, S.; Maurer, S. A.; McLaughlin, P. F.; Menger, M. F. S. J.; Mewes, J.-M.; Mewes, S. A.; Morgante, P.; Mullinax, J. W.; Oosterbaan, K. J.; Paran, G.; Paul, A. C.; Paul, S. K.; Pavošević, F.; Pei, Z.; Prager, S.; Proynov, E. I.; Rák, Á.; Ramos-Cordoba, E.; Rana, B.; Rask, A. E.; Rettig, A.; Richard, R. M.; Rob, F.; Rossomme, E.; Scheele, T.; Scheurer, M.; Schneider, M.; Sergueev, N.; Sharada, S. M.; Skomorowski, W.; Small, D. W.; Stein, C. J.; Su, Y.-C.; Sundstrom, E. J.; Tao, Z.; Thirman, J.; Tornai, G. J.; Tsuchimochi, T.; Tubman, N. M.; Veccham, S. P.; Vydrov, O.; Wenzel, J.; Witte, J.; Yamada, A.; Yao, K.; Yeganeh, S.; Yost, S. R.; Zech, A.; Zhang, I. Y.; Zhang, X.; Zhang, Y.; Zuev, D.; Aspuru-Guzik, A.; Bell, A. T.; Besley, N. A.; Bravaya, K. B.; Brooks, B. R.; Casanova, D.; Chai, J.-D.; Coriani, S.; Cramer, C. J.; Cserey, G.; DePrince, A. E.; DiStasio, R. A.; Dreuw, A.; Dunietz, B. D.; Furlani, T. R.; Goddard, W. A.; Hammes-Schiffer, S.; Head-Gordon, T.; Hehre, W. J.; Hsu, C.-P.; Jagau, T.-C.; Jung, Y.; Klamt, A.; Kong, J.; Lambrecht, D. S.; Liang, W.; Mayhall, N. J.; McCurdy, C. W.; Neaton, J. B.; Ochsenfeld, C.; Parkhill, J. A.; Peverati, R.; Rassolov, V. A.; Shao, Y.; Slipchenko, L. V.; Stauch, T.; Steele, R. P.; Subotnik, J. E.; Thom, A. J. W.; Tkatchenko, A.; Truhlar, D. G.; Van Voorhis, T.; Wesolowski, T. A.; Whaley, K. B.; Woodcock, H. L.; Zimmerman, P. M.; Faraji, S.; Gill, P. M. W.; Head-Gordon, M.; Herbert, J. M.; Krylov, A. I., Software for the frontiers of quantum chemistry: An overview of developments in the Q-Chem 5 package. *J. Chem. Phys.* **2021,** *155* (8), 084801.
57. Zheng, C.; Mao, Y.; Kozuch, J.; Atsango, A. O.; Ji, Z.; Markland, T. E.; Boxer, S. G., Electric Field Orientations in Solution and Enzyme Active Site Revealed by a Two-Directional Vibrational Probe. ChemRxiv. Cambridge: Cambridge Open Engage, 2021. Preprint.
58. Claudino, D.; Mayhall, N. J., Automatic Partition of Orbital Spaces Based on Singular Value Decomposition in the Context of Embedding Theories. *J. Chem. Theory Comput.* **2019,** *15* (2), 1053-1064.
59. Luzar, A.; Chandler, D., Hydrogen-bond kinetics in liquid water. *Nature* **1996,** *379* (6560), 55-57.
60. Böttcher, C. J. F., van Belle, O.C., Bordewijk, P., Rip, A., *Theory of Electric Polarization*. 2nd ed.; Elsevier Pub. Co.: Amsterdam, The Netherlands, 1973; Vol. 1.
61. Schneider, S. H.; Kratochvil, H. T.; Zanni, M. T.; Boxer, S. G., Solvent-Independent Anharmonicity for Carbonyl Oscillators. *J. Phys. Chem. B* **2017,** *121* (10), 2331-2338.
62. Hamm, P.; Lim, M.; Hochstrasser, R. M., Structure of the Amide I Band of Peptides Measured by Femtosecond Nonlinear-Infrared Spectroscopy. *J. Phys. Chem. B* **1998,** *102* (31), 6123-6138.

63. Wang, L.; Fried, S. D.; Markland, T. E., Proton Network Flexibility Enables Robustness and Large Electric Fields in the Ketosteroid Isomerase Active Site. *J. Phys. Chem. B* **2017,** *121* (42), 9807-9815.
64. Welborn, V. V.; Head-Gordon, T., Fluctuations of Electric Fields in the Active Site of the Enzyme Ketosteroid Isomerase. *J. Am. Chem. Soc.* **2019,** *141* (32), 12487-12492.
65. Wade, R. C.; Gabdoulline, R. R.; Lüdemann, S. K.; Lounnas, V., Electrostatic steering and ionic tethering in enzyme–ligand binding: Insights from simulations. *Proc. Natl. Acad. Sci. U.S.A.* **1998,** *95* (11), 5942.
66. Gunasekaran, K.; Pentony, M.; Shen, M.; Garrett, L.; Forte, C.; Woodward, A.; Ng, S. B.; Born, T.; Retter, M.; Manchulenko, K.; Sweet, H.; Foltz, I. N.; Wittekind, M.; Yan, W., Enhancing Antibody Fc Heterodimer Formation through Electrostatic Steering Effects: Applications to Bispecific Molecules and Monovalent IgG. *J. Biol. Chem.* **2010,** *285* (25), 19637-19646.
67. Hamm, P.; Lim, M.; DeGrado, W. F.; Hochstrasser, R. M., Stimulated Photon Echoes from Amide I Vibrations. *J. Phys. Chem. A* **1999,** *103* (49), 10049-10053.
68. Harnagea, E. I.; Jagodzinski, P. W., Infrared spectra of cyclic and non-cyclic ureas in solution: structures and interactions. *Vib. Spectrosc.* **1996,** *10* (2), 169-175.
69. Warshel, A.; Sharma, P. K.; Kato, M.; Xiang, Y.; Liu, H.; Olsson, M. H. M., Electrostatic Basis for Enzyme Catalysis. *Chem. Rev.* **2006,** *106* (8), 3210-3235.
70. Walker, T. W.; Chew, A. K.; Li, H.; Demir, B.; Zhang, Z. C.; Huber, G. W.; Van Lehn, R. C.; Dumesic, J. A., Universal kinetic solvent effects in acid-catalyzed reactions of biomass-derived oxygenates. *Energ. Environ. Sci.* **2018,** *11* (3), 617-628.